# Active RIS-aided NOMA-ISAC Network Architecture for LEO Satellite Communications

Soumen Mondal<sup>†</sup>, Keshav Singh<sup>†</sup>, Chih-Peng Li<sup>†</sup>, and Zhiguo Ding<sup>‡</sup>

<sup>†</sup>Institute of Communications Engineering, National Sun Yat-sen University, Kaohsiung, Taiwan.

<sup>‡</sup>Department of Computer and Information Engineering, Khalifa University, Abu Dhabi, UAE.

E-mail: soumen.durgapur@gmail.com, keshav.singh@mail.nsysu.edu.tw, cpli@faculty.nsysu.edu.tw, zhiguo.ding@ieee.org

Abstract—This paper analyzes the performance of a nonorthogonal multiple access (NOMA)-enabled, active reconfigurable intelligent surface (RIS)-assisted integrated sensing and communication (ISAC) system operating within a non-terrestrial network (NTN) framework. The end-to-end equivalent channel under maximum ratio transmission (MRT) beamforming is derived and modeled as a Gamma distribution. A closed-form expression for the outage probability (OP) is obtained in terms of Meijer G-functions, and the analytical findings are validated via Monte Carlo simulations. To further characterize system performance, the asymptotic expression of the OP and the associated diversity order are also derived. The effectiveness of the active RIS in mitigating multiplicative fading through signal amplification is evaluated by comparison with a conventional passive RIS scheme, revealing substantial performance improvements. Moreover, the impact of hardware impairments and channel shadowing is examined. On the sensing side, the proposed ISAC system is compared with a traditional radar in terms of beampattern gain.

Index Terms—Active RIS, Non-orthogonal multiple access, Hardware impairment, Non-terrestrial network

#### I. INTRODUCTION

O ensure global connectivity, networks increasingly integrate terrestrial and non-terrestrial infrastructures. In particular, low earth orbit (LEO) satellites (500-2000 km altitude) offer seamless coverage, long-range communication, and wide spectrum access [1]. Satellite communications (SatCom) support applications such as navigation, weather monitoring, broadcasting, and emergency services, especially when terrestrial infrastructure fails. Nonetheless, SatCom faces limitations like shadowing and signal degradation over long distances, particularly in urban areas. To mitigate these issues and improve communication with ground users, reconfigurable intelligent surfaces (RIS) have emerged as a promising solution. RIS comprises a large array of programmable elements capable of dynamically controlling the phase and amplitude of incident signals to steer their propagation direction. Traditional passive RISs experience severe performance degradation due to dou-

This work was supported by the National Science and Technology Council of Taiwan under Grants NSTC 113-2222-E-110-008-MY3 and NSTC 114-2218-E-110-005, and the Sixth Generation Communication and Sensing Research Center funded by the Higher Education SPROUT Project, the Ministry of Education of Taiwan.

ble path loss attenuation arising from the cascaded transmitter—RIS—receiver link, commonly referred to as multiplicative fading. To overcome this limitation, active RIS has been introduced, wherein each reflecting element is equipped with a low-power amplifier powered by an external source to amplify and reflect incident signals [2]. Despite these advantages, active RIS introduces increased power consumption relative to its passive counterpart.

Beyond boosting data rates, wireless communication aims to expand coverage and support massive connectivity. In this context, non-orthogonal multiple access (NOMA) facilitates simultaneous multi-user transmission via power-domain multiplexing and superposition coding [3]. At the receiver, signals are separated using successive interference cancellation (SIC), where stronger signals are decoded and subtracted prior to decoding the weaker ones. In addition to channel impairments, RF transceivers suffer from hardware impairments (HI) such as I/Q imbalance, quantization errors, phase noise, and amplifier nonlinearities, arising during up/down-conversion. Radar communication is vital in autonomous driving, surveillance, robotics, and smart traffic systems. The growing need for highresolution sensing in VR and IoT has sparked interest in radarbased solutions. Integrated sensing and communication (ISAC) unifies sensing and communication, improving spectral and energy efficiency [4]. ISAC also reduces complexity through shared processing and enables joint waveform design for better performance. Its reliance on LoS paths ensures precise sensing and enhanced security, even in satellite systems.

This study focuses on the integration of three core technologies— ISAC, active RIS, and NOMA—to address the performance challenges in next-generation wireless networks. The work in [1] addressed energy efficiency optimization for ISAC systems but was restricted to single-target detection. In contrast, [5] extended the investigation to ISAC scenarios involving multiple targets and multiple communication users. To enhance ISAC system performance, [6] exploited the RIS's ability to introduce additional LoS paths, aiming to maximize the weighted sum-rate and minimize sensing pattern error in a multi-user scenario using a passive RIS. In [7], an active RIS was introduced to support both functionalities, with joint optimization of the beamforming vector and IRS coefficients

Table I: Comparison with relevant work

Ref.	Network Type		RIS Type	Multiple ISAC		ні
	Terrestrial	NTN RIS Type		access	ISAC	111
[1]	Х	1	Passive	NOMA	Х	Х
[9]	· · · · · ·	×	Active	NOMA	×	<b>7</b>
[10]	<b>√</b>	×	Active	NOMA	X	<i>\</i>
[11]	·	_ x	Active	NOMA		X
[12]	x		Passive		X	<b>7</b>
Our work	<b>X</b>	<b>-</b>	Active	NOMA		<b>-</b>

to enhance radar SINR. On the otherside, the performance of satellite communication is enhanced using an unmanned aerial vehicle (UAV)-assisted RIS, where the UAV acts as a mobile relay, and the system is evaluated in terms of outage [8]. To support more users, multiple access techniques such as NOMA have been integrated into RIS-assisted ISAC systems [9].

From a performance analysis perpective, the closed-form and asymptotic expressions for outage probability, ergodic rate, and energy efficiency are derived for active RIS-assisted NOMA networks under HI [9]. Whereas, the paper [10] analyzes an active RIS-assisted downlink NOMA network with HI and imSIC, deriving closed-form expressions for outage probability and ergodic capacity using Meijer G-functions under transmit antenna selection. Most existing works have primarily concentrated on optimization-based designs, with limited attention given to analytical performance analysis of ISAC systems, as addressed in only a few recent studies [11]. To the best of our knowledge, active RIS-assisted NOMA-ISAC systems in NTN environments remain analytically unexplored. Motivated by this gap, we analyze such a system, with key contributions compared against existing works in Table I. Key distinctions from prior studies are as follows:

- A NOMA-ISAC scheme is analysed under HI for NTN. A
  tractable expression of the outage probability has been derived in terms of Meijer G-function to evaluate the system
  performance. We investigate the significant performance
  degradation in outage probability caused by HI.
- We derive asymptotic outage expressions in the high-SNR regime to analyze the impact of key system parameters.
   The resulting diversity order quantifies the outage decay rate and is shown to scale proportionally with the number of transmit antennas and indirectly with the number of RIS elements through the shape parameter.
- The sensing capability of the proposed ISAC system is evaluated by comparing its beampattern gain with a conventional radar system for aerial targets.

#### II. SYSTEM ARCHITECTURE AND SIGNAL MODELS

As illustrated in Fig. 1, an active RIS-assisted ISAC system is considered, wherein a LEO satellite simultaneously communicates with M ground users (GUs) using NOMA and detects T aerial targets. The active RIS consists of N reconfigurable elements arranged in a uniform planar array (UPA) configuration. The satellite is equipped with L antennas arranged in a uniform

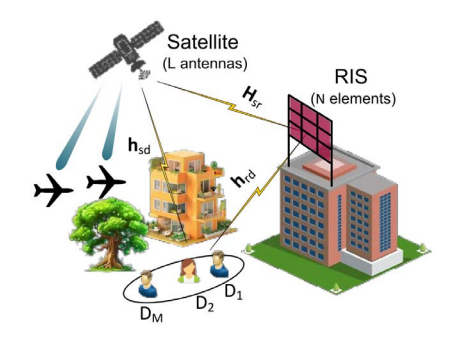


Fig. 1: Active RIS-aided NOMA-ISAC network for a LEO satellite system.

linear array (ULA), and each GU is assumed to be equipped with a single antenna. Let  $\mathcal{M} \triangleq \{1,\ldots,M\}$ ,  $\mathcal{L} \triangleq \{1,\ldots,L\}$ , and  $\mathcal{N} \triangleq \{1,\ldots,N\}$  respectively denote the set of GUs, the number of antennas at the satellite, and the number of reflecting elements at the active RIS, respectively.

## A. Signal Modeling

The ISAC system transmits a superposition of precoded sensing and communication signals from the satellite

$$\mathbf{x} = \sum_{m \in \mathcal{M}} \sqrt{a_m^c} \widetilde{\mathbf{w}}_m c_m + \sum_{t \in \mathcal{T}} \sqrt{a_t^t} \widetilde{\mathbf{v}}_t s_t, \tag{1}$$

where  $\widetilde{\mathbf{w}}_m \in \mathbb{C}^{L \times 1}, m \in \mathcal{M}$ , and  $\widetilde{\mathbf{v}}_t \in \mathbb{C}^{L \times 1}, t \in \mathcal{T}$  are the beamforming vector of the NOMA signal for the mth GU, and the beamforming vector of the tth target. The  $\{c_m, a_m^c\}$ , and  $\{s_t, a_t^t\}$  are the communication signal for the mth GU, and the tth target respectively. The dedicated sensing signal  $s_t$  and communication signal  $c_t$  are modeled as statistically independent random variables, both having zero mean and unit power, i.e.,  $\mathbb{E}\left\{\mathbf{s}\mathbf{s}^{H}\right\} = \mathbf{I}_{M+T}$  where  $\mathbf{s} = \left[c_{1}\ldots,c_{m},s_{1},\ldots,s_{t}\right]^{T} \in$  $\mathbb{C}^{M+T}$ . Let  $\delta \in (0,1)$  denote the fraction of the total transmit power  $P_T$  allocated to the communication signal. Accordingly, the communication and sensing signal powers are given by  $P_c = \delta P_T$  and  $P_s = (1 - \delta)P_T$ , respectively. The available transmit power is distributed among the communication and dedicated sensing signal  $P_c + P_t = P_T$ ,  $\sum_{m=1}^M a_m^c = 1$  and  $\sum_{t=1}^T a_t^t = 1$ . The sensing and communication signals are steered using beamforming vectors given by  $\tilde{\mathbf{w}}_m = \sqrt{P_c} \mathbf{w}_m$ and  $\widetilde{\mathbf{v}}_t = \sqrt{P_{\mathrm{t}}}\mathbf{v}_t$ , Thus, the transmit signal covariance matrix is given as  $\mathbf{R}_{\mathbf{x}} = \mathbb{E}\left[\mathbf{x}\mathbf{x}^H\right] = \sum_{m=1}^{M} \widetilde{\mathbf{w}}_m \widetilde{\mathbf{w}}_m^H +$  $\sum_{t=1}^{T} \widetilde{\mathbf{v}}_{t} \widetilde{\mathbf{v}}_{t}^{H}. \text{ Let us define } \mathbf{W} = [\mathbf{w}_{1}, \dots, \mathbf{w}_{M}, \mathbf{v}_{1}, \dots, \mathbf{v}_{T}] \in \mathbb{C}^{L \times (M+T)} \quad \xi_{s} = \mathcal{CN} \left(0, \kappa_{s}^{2} P_{T} \operatorname{diag} \left(\mathbf{W} \mathbf{W}^{H}\right)\right) \quad [13]. \quad \xi_{m} = \mathbf{w}_{1} = \mathbf{w}_{1} + \mathbf{w}_{2} = \mathbf{w}_{2} + \mathbf{w}_{3} = \mathbf{$  $\mathcal{CN}\left(0,\kappa_m^2 P_T |\mathbf{h}_{\mathrm{sd}_m}^{\mathrm{eff}}|^2\right)$  [9]. We adopt the MRT beamforming technique at the transmitter, owing to its simplicity and mathematical tractability, i.e.,  $\mathbf{w}_m = \frac{(\mathbf{h}_{\mathrm{sd}_m}^{\mathrm{eff}})^H}{\|\mathbf{h}_{\mathrm{sd}_m}^{\mathrm{eff}}\|}$ .

## B. Channel Modeling

In this section, we present the modeling of both the terrestrial and satellite communication channels characteristics.

1) Terrestrial channel: The large-scale channel power gain, denoted by  $\beta_{\mathrm{rd}_m}$ , captures the effects of path loss. It is expressed as  $\beta_{\mathrm{rd}_m} = \beta_0 d_{\mathrm{rd}_m}^{-\alpha}$ ,  $\beta_0$  represents the average channel power gain at a reference distance of  $d_0 = 1\,\mathrm{m}$ , and  $\alpha$  denotes the path-loss exponent. Next, owing to the presence of a dominant LoS component, characterized by a Rician distribution. The channel vector  $\mathbf{h}_{\mathrm{rd}_m}$  follows Rician fading with normalized average power, such that  $\mathbb{E}\{|\mathbf{h}_{\mathrm{rd}_m}|^2\} = \beta_{\mathrm{rd}_m}$ . Accordingly, the channel can be expressed as:

$$\mathbf{h}_{\mathrm{rd}_{m}} = \sqrt{\beta_{\mathrm{rd}_{m}}} \left( \sqrt{\frac{K}{K+1}} \overline{\mathbf{h}}_{\mathrm{rd}_{m}}^{\mathrm{LOS}} + \sqrt{\frac{1}{K+1}} \widetilde{\mathbf{h}}_{\mathrm{rd}_{m}}^{\mathrm{nLOS}} \right), \quad (2)$$

where,  $\widetilde{\mathbf{h}}_{\mathrm{rd}}^{\mathrm{nLOS}}$  represents the scattered component of the chan-

nel,  $\widetilde{\mathbf{h}}_{\mathrm{rd}_m}^{\mathrm{nLOS}^n} \sim \mathcal{CN}(0,\mathbf{1})$ , and K denotes the Rician K-factor. The moments of Rician faded channel given in Table IV in [4]. 2) Satellite channel: The pathloss in satellite channel can be describe as  $\mathcal{PL}_m = G_s G_g \left(\frac{c}{4\pi f_c d_m}\right)^2$ , including the free space path loss and antenna gains, where  $d_m$  is the distance between S and  $D_m$ , c is the speed of light, and  $f_c$  is the carrier frequency,  $G_g$  is the antenna gain of the GU and  $G_s = G_{\mathrm{max}} \left(\frac{J_1(w)}{2w} + 36\frac{J_3(w)}{w^3}\right)^2$  is the beam gain of the satellite. Here  $J_v(\cdot)$  denotes the first kind Bessel function of order v and  $\omega = 2.07123 \frac{\sin(\phi)}{\sin(\phi_{3dB})}$ , where  $\phi_{3dB}$  is the 3 dB beam angle,  $\phi$  is the angle between  $d_m$  and the center of

$$f_{|h_j|}(x) = 2\alpha_j e^{-(\beta_j - \delta_j)x^2} \sum_{k=0}^{m_j - 1} \frac{(-1)^k (1 - m_j)_k (\delta_j)^k x^{2k+1}}{(k!)^2}.$$
 (3)

satellite beam, and  $G_{\max}$  is the maximum gain of the satellite beam. The shadowed Rician distribution provides an effective

characterization of satellite-to-GU links. The corresponding

probability density function (PDF) is given by [14]:

The CDF of the shadowed Rician channel can be expressed as

$$F_{|h_{j}|^{2}}(x) = 1 - \alpha_{j}e^{-(\beta_{j} - \delta_{j})x}$$

$$\times \sum_{k=0}^{m_{j}-1} \sum_{l=0}^{k} \frac{(-1)^{k}(1 - m_{j})_{k}(\delta_{j})^{k}}{k!l!} x^{l}(\beta_{j} - \delta_{j})^{-(k-l+1)}.$$
(4)

where  $\alpha_j = \frac{1}{2b_j} \left(\frac{2b_j m_j}{2b_j m_j + \Omega_j}\right)^{m_j}$ ,  $\beta_j = \frac{1}{2b_j}$ ,  $\delta_j = \frac{\Omega_j}{2(2b_i^2 m_j + b_i \Omega_j)}$ . The parameter  $\Omega_i$  denotes the average power of the LoS component, while  $b_j$  represents the average power of the multipath component. From (3), we can derive nth the moments of  $|h_j|$  as

$$\mu_j^{(n)} = 2\alpha_j \sum_{k=0}^{m_j - 1} \frac{(-1)^k (1 - m_j)_k (\delta_j)^k \Gamma\left(k + 1 + \frac{n}{2}\right)}{\left(k!\right)^2 2(\beta_j - \delta_j)^{k+1 + \frac{n}{2}}}.$$
 (5)

C. Received signal analysis

The mth GU receives a direct signal, a cascaded signal via active RIS, RIS-induced noise, and AWGN, all affected by

transceiver HI, and the received signal is expressed as:

$$y_{m} = \sqrt{P_{s}} (\mathbf{h}_{sd_{m}}^{\text{dir}} + \mathbf{h}_{rd_{m}} \mathbf{\Phi} \mathbf{H}_{sr}) (\mathbf{x} + \xi_{s}) + \mathbf{h}_{rd_{m}} \mathbf{\Phi} \mathbf{n}_{r} + \xi_{m} + \mathbf{n}_{m},$$

$$= \sqrt{P_{s}} \mathbf{h}_{sd_{m}}^{\text{eff}} (\mathbf{x} + \xi_{s}) + \mathbf{h}_{rd_{m}} \mathbf{\Phi} \mathbf{n}_{r} + \xi_{m} + \mathbf{n}_{m}. \tag{6}$$

The matrix  $\Phi = \operatorname{diag}\left(\eta_1 e^{j\phi_1}, \ldots, \eta_N e^{j\phi_N}\right) \in \mathbb{C}^{N \times N}$ , the parameters  $\eta_n$   $(\eta_n > 1)$  and  $\phi_n$  denote the amplitude amplification factor and the phase shift introduced by the nth RIS reflecting element, respectively. The noise for amplification in the active RIS is modeled as  $\mathbf{n_r} \sim \mathcal{CN}(\mathbf{0_N}, \sigma_r^2 \mathbf{I_N}) \in \mathbb{C}^{N \times 1}$ . Additionally, the additive white Gaussian noise (AWGN) at the mth GU is denoted by  $\mathbf{n}_m \sim \mathcal{CN}(0, \sigma_m^2)$ . It is assumed that all active RIS elements share a uniform amplification factor, i.e.,  $\eta_1 = \eta_2 = \ldots = \eta_N = \eta$ ,  $\Phi = \eta \Theta$ , where  $\Theta = \operatorname{diag}(e^{j\phi_1}, \ldots, e^{j\phi_N})$  and  $a_1^c > a_2^c > \ldots > a_M^c$ .

1) End-to-end channel Modeling: The effective channel between the lth satellite antenna and the mth GU is represented as  $\left|h_{\mathrm{s_l d_m}}^{\mathrm{eff}}\right| = \left|h_{\mathrm{s_l d_m}}^{\mathrm{dir}}\right| + \sum_{n=1}^N \eta_n e^{j\theta_n} \left|h_{\mathrm{s_l r_n}}\right| \left|h_{\mathrm{r_n d_m}}\right|$  where  $\theta_n = \angle h_{\mathrm{s_l d_m}}^{\mathrm{dir}} - \angle h_{\mathrm{s_l r_n}} - \angle h_{\mathrm{r_n d_m}}$ ,  $h_{\mathrm{s_l r_n}}^{\mathrm{dir}}$  denotes the direct channel,  $h_{\mathrm{s_l r_n}}$  and  $h_{\mathrm{r_n d_m}}$  represent the channels from lth antenna of the satellite to the nth RIS element and from the nth RIS element to the mth GU, respectively. Here,  $\left|h_{\mathrm{s_l l_m}}^{\mathrm{dir}}\right|$  and  $\left|h_{\mathrm{s_l r_n}}\right|$  are the shadow rician faded direct link from lth antenna of the satellite to RIS,  $\left|h_{\mathrm{rd_m}}\right|$  are the Rician faded channel from active-RIS to mth GU, respectively. We assume that  $\mathcal{A}_{l,m} \triangleq \left|h_{\mathrm{s_l l_m}}^{\mathrm{dir}}\right|$ ,  $\mathcal{B}_{l,m} \triangleq \sum_{n=1}^N \left|h_{\mathrm{s_l r_n}}\right| \left|h_{\mathrm{r_n d_m}}\right|$ ,  $\mathcal{C}_{l,n} \triangleq \left|h_{\mathrm{s_l r_n}}\right|$ ,  $\mathcal{D}_{n,m} \triangleq \left|h_{\mathrm{r_n d_m}}\right|$ , and  $\mathcal{W}_m \triangleq \sum_{n=1}^N \left|h_{\mathrm{r_n d_m}}\right|$ . In this paper, an optimal phase shift is considered, hence  $Z_{l,m} = \mathcal{A}_{l,m} + \eta \mathcal{B}_{l,m}$ .

The mean of the satellite to mth GU Rician faded channel is  $\mu_{\mathcal{A}_{l,m}}^{(1)} = \mathbb{E}\left\{|h_{\mathbf{s}_l\mathbf{d}_m}|\right\} = \mathbb{E}\left\{\mathcal{A}_{l,m}\right\}$  can be obtained by putting n=1 in eq. (5). Since  $|h_{\mathbf{s}_l\mathbf{r}_n}|$  and  $|h_{\mathbf{r}_n\mathbf{d}_m}|$  are i.i.d RV. The  $\mathcal{B}_{l,m}$  is the sum of N i.i.d RVs. Therefore, with help of CLT, the distribution of  $\mathcal{B}_{l,m}$  approaches Gaussian distributed with mean  $\mu_{\mathcal{B}_{l,m}}^{(1)} = \mathbb{E}\left\{\mathcal{B}_{l,m}\right\} = N\mu_{\mathrm{sr}}^{(1)}\mu_{\mathrm{rd}_m}^{(1)}$ . The first moment of  $Z_{l,m}$  is given as  $\mathbb{E}\left\{Z_{l,m}\right\} = \mathbb{E}\left\{\mathcal{A}_{l,m}\right\} + \eta\mathbb{E}\left\{\mathcal{B}_{l,m}\right\} = \mu_{\mathrm{sd}_m} + \eta N\mu_{\mathrm{sr}}\mu_{\mathrm{rd}_m}$  Further, the second moment of  $\mathcal{B}_{l,m}$  is given by

$$\mu_{\mathcal{B}_{l,m}}^{(2)} = N \mu_{\rm sr}^{(2)} \mu_{\rm rd_m}^{(2)} + N(N-1) \left( \mu_{\rm sr}^{(1)} \mu_{\rm rd_m}^{(1)} \right)^2. \tag{7}$$

Furthermore, the third moment of  $\mathcal{B}_{l,m}$  is given by

$$\mu_{\mathcal{B}_{l,m}}^{(3)} = N \mu_{\text{sr}}^{(3)} \mu_{\text{rd}_{\text{m}}}^{(3)} + 3N \left(N - 1\right) \mu_{\text{sr}}^{(2)} \mu_{\text{rd}_{\text{m}}}^{(2)} \mu_{\text{sr}}^{(1)} \mu_{\text{rd}_{\text{m}}}^{(1)} + N \left(N - 1\right) \left(N - 2\right) \left(\mu_{\text{sr}}^{(1)} \mu_{\text{rd}_{\text{m}}}^{(1)}\right)^{3}. \tag{8}$$

Finally, the fourth moment of  $\mathcal{B}_{l,m}$  is given in (9) as:

$$\begin{split} \mu_{\mathcal{B}_{l,m}}^{(4)} = & N \mu_{\text{sr}}^{(4)} \mu_{\text{rd}_{m}}^{(4)} + 4N \left(N-1\right) \mu_{\text{sr}}^{(3)} \mu_{\text{rd}_{m}}^{(3)} \mu_{\text{rd}_{m}}^{(1)} \mu_{\text{rd}_{m}}^{(1)} \\ & + 3N \left(N-1\right) \left(\mu_{\text{sr}}^{(2)} \mu_{\text{rd}_{m}}^{(2)}\right)^{2} \\ & + 6N \left(N-1\right) \left(N-2\right) \mu_{\text{sr}}^{(2)} \mu_{\text{rd}_{m}}^{(2)} \left(\mu_{\text{sr}}^{(1)} \mu_{\text{rd}_{m}}^{(1)}\right)^{2} \\ & + N \left(N-1\right) \left(N-2\right) \left(N-3\right) \left(\mu_{\text{sr}}^{(1)} \mu_{\text{rd}_{m}}^{(1)}\right)^{4}. \end{split} \tag{9}$$

Let A be a gamma-distributed RV, and its CDF is given by

$$F_{\mathbb{A}}(x) = \frac{1}{\Gamma(\Theta_{\mathbb{A}})} \gamma\left(\Theta_{\mathbb{A}}, \frac{x}{\Psi_{\mathbb{A}}}\right), \tag{10}$$

where  $\mathbb{A} = \{\Gamma_m, \chi_m\}$ . The term  $\Theta_{\mathbb{A}}$  and  $\Psi_{\mathbb{A}}$  denote shape parameter and scale parameter of A respectively and given by

$$\Theta_{\mathbb{A}} = \frac{\left[\mathbb{E}\left\{\mathbb{A}\right\}\right]^{2}}{\mathbb{E}\left\{\mathbb{A}^{2}\right\} - \left[\mathbb{E}\left\{\mathbb{A}\right\}\right]^{2}}, \ \Psi_{\mathbb{A}} = \frac{\mathbb{E}\left\{\mathbb{A}^{2}\right\} - \left[\mathbb{E}\left\{\mathbb{A}\right\}\right]^{2}}{\mathbb{E}\left\{\mathbb{A}\right\}}.$$
(11)

Let  $\chi_m = |\mathbf{h}_{\mathrm{rd_m}} \mathbf{\Phi} \mathbf{n}_{\mathrm{r}}|^2 \sim \mathcal{G}\left(\Theta_{\chi_m}, \Psi_{\chi_m}\right), \ \mathbb{E}\left\{\chi_m\right\} = \eta^2 N \beta_{\mathrm{rd_m}} \sigma_{\mathrm{r}}^2, \ \mathbb{E}\left\{\chi_m^2\right\} = N \eta^4 \mu_{\mathrm{rd_m}}^{(4)} + N \eta^4 (N-1) \{\mu_{\mathrm{rd_m}}^{(2)}\}^2.$  The effective channel gain from the satellite to the mth GU,

employing MRT beamforming, is expressed as  $\|\mathbf{h}_{\mathrm{sd}_{m}}^{\mathrm{eff}}\|^{2} = \Gamma_{m} = \sum_{l=1}^{L} \Gamma_{m,l} = \sum_{l=1}^{L} Z_{m,l}^{2}$ . The corresponding the shape parameter of  $\Gamma_{m}$  is  $\Theta_{\Gamma_{m}} = \sum_{l=1}^{L} \Theta_{\Gamma_{m,l}}$  and scale parameter remains same  $\Psi_{\Gamma_m}=\Psi_{\Gamma_{m,l}}$  [15]. By substituting the shape and scale parameters into (10), the CDFs of  $\Gamma_m$ ,  $\chi_m$  can be achieved. It is essential to compute the first and second moments of  $\Gamma_{m,l}$  to derive the expressions for  $\Theta_{\Gamma_{m,l}}$  and  $\Psi_{\Gamma_{m,l}}$ as presented in (12) and (13), respectively.

$$\mu_{\Gamma_{m,l}}^{(1)} = \mathbb{E}\left\{\mathcal{A}_{l,m}^{2}\right\} + 2\eta \mathbb{E}\left\{\mathcal{A}_{l,m}\right\} \mathbb{E}\left\{\mathcal{B}_{l,m}\right\} + \eta^{2} \mathbb{E}\left\{\mathcal{B}_{l,m}^{2}\right\},$$

$$= \mu_{\mathrm{sd}_{m}}^{(2)} + 2N\eta \mu_{\mathrm{sd}_{m}}^{(1)} \mu_{\mathrm{IU}_{m}}^{(1)} + N\eta^{2} \mu_{\mathrm{sr}}^{(2)} \mu_{\mathrm{rd}_{m}}^{(2)}$$

$$+ N(N-1)\eta^{2} \left(\mu_{\mathrm{sr}}^{(1)} \mu_{\mathrm{rd}_{m}}^{(1)}\right)^{2}.$$
(12)

The second-order moment of  $\Gamma_{m,l}$ , denoted by  $\mu_{\Gamma_{m,l}}^{(2)} =$  $\mathbb{E}\left\{\Gamma_{m,l}^2\right\}=\mathbb{E}\left\{Z_{m,l}^4\right\}\!$ , is derived based on the results provided in (7)–(9), and its expression is given as

$$\mu_{\Gamma_{m,l}}^{(2)} = \mu_{\mathcal{A}_{l,m}}^{(4)} + \eta^4 \mu_{\mathcal{B}_{l,m}}^{(4)} + 4\eta \mu_{\mathcal{A}_{l,m}}^{(3)} \mu_{\mathcal{B}_{l,m}}^{(1)} + 4\eta^3 \mu_{\mathcal{A}_{l,m}}^{(1)} \mu_{\mathcal{B}_{l,m}}^{(3)} + 6\eta^2 \mu_{\mathcal{A}_{l,m}}^{(2)} \mu_{\mathcal{B}_{l,m}}^{(2)}.$$
(13)

By substituting the required moments from (5) into (12) and (13), the shape and scale parameters can be determined. Subsequently, the CDF expression can be obtained using (10).

#### III. PERFORMANCE ANALYSIS

The SINR corresponding to the kth signal received at the mth GU in the presence of HI is provided as [9].

$$\gamma_m^{(k)} = \frac{P_c \|\mathbf{h}_{\mathrm{sd}_m}\|^2 a_k^c}{P_c \|\mathbf{h}_{\mathrm{sd}_m}\|^2 \sum_{j=k+1}^M a_j^c + P_t \|\mathbf{h}_{\mathrm{sd}_m}\|^2 + P_T \|\mathbf{h}_{\mathrm{sd}_m}\|^2 \kappa_{\mathrm{h}}^2 + N_{Tot}},$$
(14)

where  $N_{Tot} = \left\| \mathbf{h}_{\mathrm{rd}_m}^{\mathrm{H}} \mathbf{\Phi} \right\|^2 \sigma_I^2 + \sigma_k^2$ ,  $\kappa_{\mathrm{h}}^2 = (\kappa_s^2 + \kappa_m^2)$ . The CDF of the effective received SINR corresponding to  $x_m$  at the mth GU is given as follows:

$$F_{\widetilde{\gamma}_{m}^{(m)}}(\gamma_{th}) = \mathcal{P}_{r} \left\{ \min_{k=1,2,\dots,m} \gamma_{m}^{(k)} < \gamma_{th} \right\},$$

$$= \mathcal{P}_{r} \left( \frac{\Lambda_{1} \Gamma_{m}}{\Lambda_{2} \chi_{m} + 1} < \widetilde{\Delta}_{m}^{(m)} \right) = F_{W} \left( \widetilde{\Delta}_{m}^{(m)} \right),$$

$$(15)$$

where, 
$$W = \frac{\mathcal{A}_1 \Gamma_m}{\mathcal{A}_2 \chi_m + 1}$$
,  $\Lambda_1 = \frac{1}{\sigma_k^2 + P_T \Omega_m}$ , and  $\Lambda_2 = \frac{\kappa \sigma_I^2}{\sigma_k^2 + P_T \Omega_m}$ ,  $\widetilde{\Delta}_m^{(m)} = \max_{k=1,\dots,m} \left(\Delta_m^{(k)}\right)$ , 
$$\Delta_m^{(k)} = \frac{\gamma_{th}}{\left(\delta a_k^c - \delta \sum\limits_{j=k+1}^M a_j^c - (1-\delta) - \kappa_h^2\right) P_T}.$$

Theorem 1: The closed form expression for  $F_W\left(\widetilde{\Delta}_m^{(m)}\right)$  is given in (17), shown at the top of the next page. The identity  $\gamma\left(a,z\right)=G_{1,2}^{1,1}\left(z\left|_{a,0}^{1}\right.\right)$  and  $e^{-z}z^{b}=G_{0,1}^{1,0}\left(z\left|b\right.\right)$  [16, Eq. (7.34.0228.01)] are employed in step (a). In step (b), a change of variable is applied, while step (c) makes use of the identity provided in [16, Eq. (07.34.21.0082.01)] to derive the closedform expression as follows:

$$\begin{split} F_{W}\left(w\right) &= P\left(\frac{\Lambda_{1}X}{\Lambda_{2}Y+1} < w\right), \\ \overset{(a)}{=} \int\limits_{y=0}^{\infty} \mathcal{C}_{1}G_{1,2}^{1,1}\left(\frac{w\left(\Lambda_{2}y+1\right)}{\Lambda_{1}\psi_{\Gamma_{m}}} \Big|_{\Theta_{\Gamma_{m}},0}^{1}\right) G_{0,1}^{1,0}\left(\frac{y}{\psi_{\chi_{m}}} \Big|_{\Theta_{\chi_{m}}-1}^{-}\right) dy, \\ \overset{(b)}{=} \int\limits_{t=0}^{\infty} \frac{\mathcal{C}_{1}\Lambda_{1}\psi_{\Gamma_{m}}}{w\Lambda_{2}} G_{1,2}^{1,1}\left(t+\frac{w}{\mathcal{C}_{2}}\Big|_{\Theta_{\Gamma_{m}},0}^{1}\right) G_{0,1}^{1,0}\left(\frac{\mathcal{C}_{3}t}{w}\Big|_{\Theta_{\chi_{m}}-1}^{-}\right) dy, \\ \overset{(c)}{=} \frac{\mathcal{C}_{1}\mathcal{C}_{2}}{w\Lambda_{2}} \sum_{k=0}^{\infty} \frac{1}{k!} \left(-\frac{w}{\mathcal{C}_{2}}\right)^{k} G_{3,3}^{2,2}\left(\frac{\mathcal{C}_{3}}{w}\Big|_{\Theta_{\chi_{m}}-1,k-1,k}^{0}\right), \end{split}$$
(16)

where  $C_1 = \frac{1}{\psi_{\chi_m} \Gamma(\Theta_{\Gamma_m}) \Gamma(\Theta_{\chi_m})}$ ,  $C_2 = \Lambda_1 \psi_{\Gamma_m}$ , and  $C_3 = \frac{\Lambda_1 \psi_{\Gamma_m}}{\Lambda_2 \psi_{\chi_m}}$ . The final expressions for CDF of W can be expressed as (17).

### A. Outage Probability

1) Exact Analysis: In a NOMA-based network, each GU receives a superposed signal from the satellite and performs SIC, where outage occurs if it fails to decode any stronger interfering signal or its own, leading to the following outage condition:

$$\mathcal{O}^{(m)} = \mathcal{P}_r \left\{ \widetilde{\gamma}_m^{(m)} < \gamma_{\text{th}} \right\} = F_{\widetilde{\gamma}_m^{(m)}} \left( \gamma_{\text{th}} \right), \tag{18}$$

where  $F_{\widetilde{\gamma}_{n}^{(m)}}$  is CDF of the SINR of mth signal at mth GU. By substituting the closed-form expression of the CDF of Wfrom (17) into (15), and subsequently into (18), the closed-form expression for the outage probability is derived.

2) Asymptotic Analysis: To determine the diversity order, the outage probability is examined in the high-SNR regime as  $P_T \to \infty$ , with the corresponding asymptotic expression is:

$$\mathcal{O}_{P_T \to \infty}^{(m)} = F_{\widetilde{\gamma}_m^{(m)}}^{\infty} \left( \gamma_{\text{th}} \right), \tag{19}$$

where  $F_{\widetilde{\gamma}^{(m)}}^{\infty}\left(\gamma_{\mathrm{th}}\right)$  denotes the CDF of received SINR in asymptotic regime. When  $P_{\rm T} \to \infty$ ,  $F_{\widetilde{\alpha}^{(m)}}^{\infty} (\gamma_{\rm th})$  can be derived from (17) using [16, eq. 07.34.06.0044.01] and expressed as

$$F_{\gamma_m^{(m)}}^{\infty}(\gamma_{\text{th}}) = \frac{\mathcal{C}_1 \mathcal{C}_2 \Gamma(\Theta_{\Gamma_m}) \Gamma(\Theta_{\chi_m})}{\mathcal{C}_3 \Lambda_2} + \frac{\mathcal{C}_1 \mathcal{C}_2 \Gamma(\Theta_{\Gamma_m} + \Theta_{\chi_m})}{(\mathcal{C}_3)^{1 - \Theta_{\Gamma_m}} \Lambda_2 \Theta_{\Gamma_m}} \left( \Delta_m^{(m)} \right)^{\Theta_{\Gamma_m}}$$
(20)

$$F_{W}\left(\widetilde{\Delta}_{m}^{(m)}\right) = \frac{\Lambda_{1}\psi_{\Gamma_{m}}}{\psi_{\chi_{m}}\Gamma\left(\Theta_{\Gamma_{m}}\right)\Gamma\left(\Theta_{\chi_{m}}\right)\widetilde{\Delta}_{m}^{(m)}\Lambda_{2}} \sum_{k=0}^{\infty} \frac{1}{k!} \left(-\frac{\widetilde{\Delta}_{m}^{(m)}}{\Lambda_{1}\psi_{\Gamma_{m}}}\right)^{k} G_{3,3}^{2,2} \left(\frac{\Lambda_{1}\psi_{\Gamma_{m}}}{\widetilde{\Delta}_{m}^{(m)}\Lambda_{2}\psi_{\chi_{m}}}\right| \begin{array}{c} 0, k - \Theta_{\Gamma_{m}}, k \\ \Theta_{\chi_{m}} - 1, k - 1, k \end{array}\right). \tag{17}$$

where 
$$C_1 = \frac{1}{\psi_{\chi_m}\Gamma(\Theta_{\Gamma_m})\Gamma(\Theta_{\chi_m})}$$
,  $C_2 = \Lambda_1\psi_{\Gamma_m}$ ,  $C_3 = \frac{\Lambda_1\psi_{\Gamma_m}}{\Lambda_2\psi_{\chi_m}}$ , and  $\{a_1, a_2, a_3\} = \{0, -\Theta_{\Gamma_m}, 0\}$ ,  $\{b_1, b_2, b_3\} = \{\Theta_{\chi_m} - 1, -1, 0\}$ .

3) Diversity Order (DO): In (20), the first term is a constant, while the second term is a function of  $(P_T)^{-\Theta_{\Gamma_m}}$ . The second term is considered dominant as it primarily governs the rate at which the outage probability decays. It is observed that  $\mathcal{O}_{P_T \to \infty}^{(m)}$  decreases proportionally to  $P_T^{-\Theta_{\Gamma_m}}$ , which is consistent with the results reported in [4]. Therefore, the diversity order  $\mathcal{D}$  of the system is identified as  $\Theta_{\Gamma_m} = \sum_{l=1}^L \Theta_{\Gamma_m,l}$ .

Remark 1: The DO proportional to L and  $\Omega_{\tau_{m,l}}$ , leading to a reduction in OP as L increases. and improves with more RIS elements. The amplification gain also increases the diversity.

#### B. Sensing Model

This work considers a monostatic ISAC setup where the satellite transmits a combined probing and communication signal, with target reflections arriving via multipath. Beamforming is used to enhance the beampattern toward target directions, and sensing is performed based on the transmit beampattern gain steered toward angle  $\phi_t$ ,  $t \in \mathcal{T}$  is given by

$$\mathcal{P}(\phi_t) = \widetilde{\beta}_t \mathbb{E}\left\{ \left| \mathbf{a}_{tx}^H (\phi_t) \mathbf{x} \right|^2 \right\} = \widetilde{\beta}_t \mathbf{a}_{tx}^H (\phi_t) \mathbf{R}_{\mathbf{x}} \mathbf{a}_{tx} (\phi_t). \quad (21)$$

Here  $\mathbf{a}_{\mathrm{rx}} \in \mathbb{C}^{L \times 1}$ ,  $\mathbf{a}_{\mathrm{tx}} \in \mathbb{C}^{L \times 1}$ , and  $\mathbf{x} \in \mathbb{C}^{L \times 1}$ ,  $\widetilde{\beta}_t$  denotes the radar cross section (RCS) of the tth target, and  $\mathbf{R}_{\mathbf{x}} = \mathbb{E}\left\{\mathbf{x}\mathbf{x}^H\right\}$  is the transmit signal covariance matrix. The target response vector is given by  $\mathbf{h}_t = \sqrt{\widetilde{\beta}_t}\mathbf{a}_{tx}(\phi_t)$ . The transmit steering vectors  $\mathbf{a}_{tx}\left(\phi_t\right) = \left[1, e^{-j\frac{2\pi d_t}{\lambda}\sin(\phi_t)}, \ldots, e^{-j\frac{2\pi d_t}{\lambda}(L-1)\sin(\phi_t)}\right]^T \in \mathbb{C}^{L \times 1}$ . The angles  $(\theta_l, \varphi_l)$  represent the azimuth and elevation angles of departure (AoDs) from the RIS toward the target. It is assumed that  $\phi_t$  and  $\widetilde{\beta}_t$  are estimated at the satellite to enable the design of an optimal transmit signal for detecting the target of interest. Accordingly, the total sensing power across T targets is expressed as  $\mathcal{P}_{\mathrm{sum}} = \sum_{t \in \mathcal{T}} \mathcal{P}(\phi_t)$ .

#### IV. SIMULATION RESULTS

We present analytical results to demonstrate the impact of various parameters on system performance. Unless otherwise specified, all simulation parameters are listed in Table II.

To evaluate the performance advantage of active RIS over passive RIS, the outage probability under various imperfect CSI scenarios is presented in Fig. 2. It can be observed that the outage probability decreases exponentially for both users,  $D_1$  and  $D_2$ . Due to higher power allocation,  $D_1$  achieves a lower outage probability compared to  $D_2$ . The results clearly demonstrate that the active RIS-assisted scheme significantly outperforms its passive counterpart. This performance gain is

Table II: System Parameters.

Symbol	Value	Symbol	Value	Symbol	Value		
$a_1^c$	0.8	$\sigma_m^2$	-80 dBm	N	36		
$a_2^c$	0.2	$\sigma_{\rm r}^2 = 4\sigma_m^2$	-74 dBm	L	2		
δ	0.9	$R_{ m th}$	1 bps/Hz	$\kappa_{ m h}$	0.01		
K	5	$G_g$	31.2 dBi	M	2		
BS	(0,0) m	$G_{\max}$	37.1 dBi	ζ	0.001		
$d_1 = d_2$	1000 km	$D_{ m RIS}$	(0,0) m	$\epsilon$	0.95		
$D_1$	(15,50) m	$D_2$	(10,30) m	$ ho_{ m t}$	25 dBm		
AS: {1	$f_c$	3 GHz					
HS: {m	$K_p$	5					
AS: Average Shadowing HS: Heavy Shadowing							

AS: Average Shadowing, HS: Heavy Shadowing.

attributed to the ability of active RIS to mitigate the impact of multiplicative fading by amplifying the incident signal. Furthermore, the steeper slope in the asymptotic outage curve of the active RIS scheme, compared to that of passive RIS, indicates an improvement in diversity, which stems from the amplification gain enhancing the effective channel. Mathematically, all moments of the effective channel distribution are improved with increasing amplification gain, consistent with the observation made in *Remark 1*.

Fig. 3 illustrates the outage probability as a function of the transmit SNR under both perfect and imperfect SIC, as well as varying levels of HI. It is observed that the outage probability increases across all scenarios with higher transmit power. In the case of imperfect SIC, the receiver fails to completely cancel the common signal, resulting in residual interference that degrades the received SNR and increases the outage probability. Since  $D_1$  treats its own signal as the desired signal and considers the other signal as interference, it does not perform SIC; hence, the SIC imperfection does not affect  $D_1$ 's performance. Moreover, the outage performance of  $D_2$  deteriorates with increasing levels of SIC imperfection. Additionally, the presence of HIs further degrades the outage performance for all users.

Fig. 4 illustrates that the outage probability decreases with increasing transmit SNR. The network exhibits improved outage performance under average shadowing conditions compared to heavy shadowing. Due to lower power allocation to  $D_2$ , it experiences a higher outage probability than  $D_1$ . Moreover, the asymptotic curves reveal a steeper decay under average shadowing, aligning well with the theoretical analysis.

Fig. 5 illustrates the beampatterns of the active RIS-assisted ISAC system with L=4 and L=8. In this setup, three targets are assumed to be located at direction angles of  $-60^{\circ}$ ,  $0^{\circ}$  and  $45^{\circ}$ . Additionally, the communication users are positioned at  $30^{\circ}$  and  $70^{\circ}$  as depicted in Fig. 6. As observed from the figure, the main beam of each beampattern is directed toward its respective target. In traditional radar, the entire

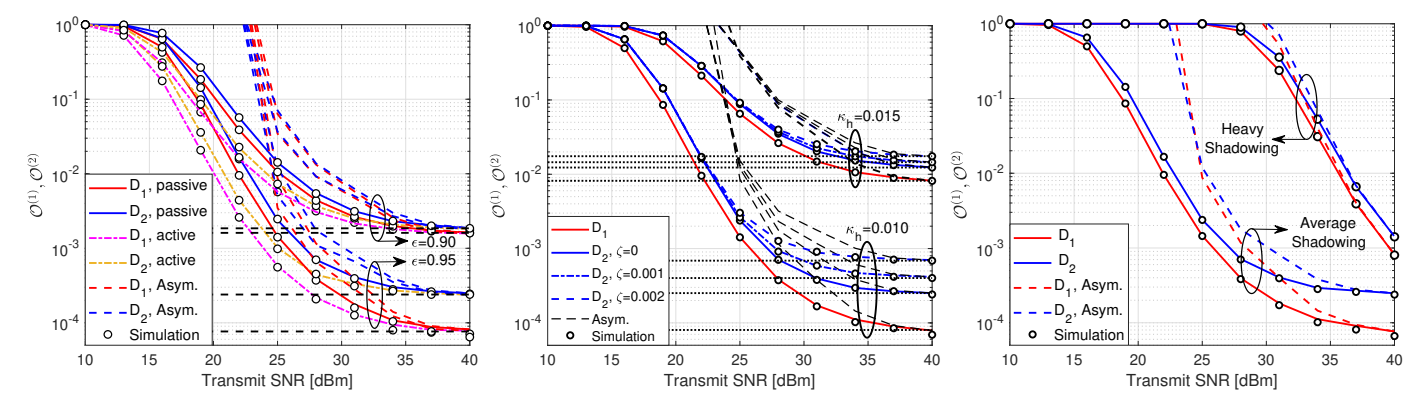


Fig. 2: Outage probability comparison for active and passive RIS Vs transmit SNR under imCSI.

Fig. 3: Outage Vs transmit SNR for different HI and imSIC

Fig. 4: Outage Vs transmit SNR under heavy and average shadowing.

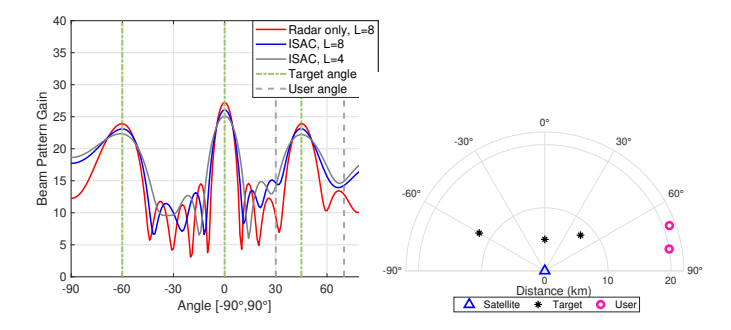


Fig. 5: Transmit beampattern gain.

Fig. 6: Layout of targets and GUs.

transmit power is dedicated to target detection, resulting in stronger power concentration in the directions of the targets compared to the ISAC system. In contrast, the ISAC framework allocates a portion of the transmit power for communication, thereby slightly reducing the power dedicated to target sensing. Moreover, increasing the number of transmit antennas at the satellite leads to a noticeable reduction in sidelobe levels.

## V. CONCLUSION

The paper presented a performance analysis of a NOMA-enhanced active RIS-assisted ISAC system under an NTN framework. A closed-form expression for the outage probability was derived based on the end-to-end equivalent channel, modeled as a Gamma distribution using the CLT and the method of moments under MRT beamforming, with validation through Monte Carlo simulations. Extensive numerical results demonstrate that the active RIS scheme achieves significant performance gains compared to the baseline passive counterpart by mitigating multiplicative fading through signal amplification. On the sensing side, the proposed ISAC system achieved more directional beampattern gain compared to conventional radar systems for aerial targets.

#### REFERENCES

W. U. Khan et al., "RIS-assisted energy-efficient LEO satellite communications with NOMA," *IEEE Trans. Green Commun. Netw.*, vol. 8, no. 2, pp. 780–790, Jun. 2023.

- [2] S. Mondal, K. Singh, C.-P. Li, and Z. Ding, "Mixed FSO/active IRS-aided MISO NOMA communication with imperfect CSI and SIC," *IEEE Internet Things J.*, vol. 12, no. 1, pp. 623–636, Jan. 2025.
- [3] D. Bepari, S. Mondal, A. Chandra, R. Shukla, Y. Liu, M. Guizani, and A. Nallanathan, "A survey on applications of cache-aided NOMA," *IEEE Commun. Surveys Tuts.*, vol. 25, no. 3, pp. 1571–1603, thirdquarter 2023.
- [4] S. Mondal, K. Singh, C. Pan, and C.-P. Li, "Performance Analysis of STAR-IRS-aided MISO-ISAC Systems with Multiple Targets: A Rate-Splitting Approach," *IEEE Trans. Commun.*, Early access 2025.
- [5] C. Meng, Z. Wei, D. Ma, W. Ni, L. Su, and Z. Feng, "Multi-objective optimization-based transmit beamforming for multi-target and multi-user MIMO-ISAC systems," *IEEE Internet Things J.*, vol. 11, no. 18, pp. 29 260–29 274, Sep. 2024.
- [6] J. Chen, K. Wu, J. Niu, Y. Li, P. Xu, and J. A. Zhang, "Spectral and energy efficient waveform design for RIS-assisted ISAC," *IEEE Trans. Commun.*, vol. 73, no. 1, pp. 158–172, Jan. 2025.
- [7] Z. Yu, H. Ren, C. Pan, G. Zhou, B. Wang, M. Dong, and J. Wang, "Active RIS aided ISAC systems: Beamforming design and performance analysis," *IEEE Trans. Commun.*, vol. 72, no. 3, pp. 1578–1595, 2024.
- [8] K. Guo and K. An, "On the performance of RIS-assisted integrated satellite-UAV-terrestrial networks with hardware impairments and interference," *IEEE Wireless Commun. Lett.*, vol. 11, no. 1, pp. 131–135, Jan. 2022.
- [9] X. Yue, M. Song, C. Ouyang, Y. Liu, T. Li, and T. Hou, "Exploiting active ris in noma networks with hardware impairments," *IEEE Trans.* Veh. Technol., vol. 73, no. 6, pp. 8207–8221, 2024.
- [10] D. Kumar, C. K. Singh, O. L. A. López, V. Bhatia, and M. Latva-aho, "Performance Analysis of Active RIS-Assisted Downlink NOMA With Transmit Antenna Selection," *IEEE Trans. Veh. Technol.*, vol. 74, no. 5, pp. 7774–7791, May 2025.
- [11] A. S. Parihar, K. Singh, V. Bhatia, C.-P. Li, and T. Q. Duong, "Performance analysis of NOMA enabled active RIS-aided MIMO heterogeneous IoT networks with integrated sensing and communication," *IEEE Internet Things J.*, vol. 11, no. 17, pp. 28137–28152, Sep. 2021.
- [12] F. Zhou, K. Guo, G. Huang, X. Li, E. K. Markakis, I. Politis, and M. Asif, "Performance evaluations for ris-aided satellite aerial terrestrial integrated networks with link selection scheme and practical limitations," *IEEE Trans. Netw. Serv. Manag.*, Early access 2024.
- [13] E. Björnson, J. Hoydis, M. Kountouris, and M. Debbah, "Massive MIMO systems with non-ideal hardware: Energy efficiency, estimation, and capacity limits," *IEEE Trans. Inf. Theory*, vol. 60, no. 11, pp. 7112–7139, 2014.
- [14] X. Yue et al., "Outage behaviors of NOMA-based satellite network over shadowed-rician fading channels," *IEEE Trans. Veh. Technol.*, vol. 69, no. 6, pp. 6818–6821, 2020.
- [15] D. Lee, "Secrecy analysis of relay-user selection in AS-AF systems over nakagami fading channels," *IEEE Trans. Veh. Technol.*, vol. 70, no. 3, pp. 2378–2388, Mar. 2021.
- [16] Wolfram Research Inc., Mathematica Edition [Online]. Available at https://functions.wolfram.com/HypergeometricFunctions/MeijerG/.